

Precision calculations of nucleon charges g_A , g_S , g_T

Rajan Gupta* †

Theoretical Division, Los Alamos National Laboratory, Los Alamos, NM 87545, USA

E-mail: rajan@lanl.gov

Tanmoy Bhattacharya

Theoretical Division, Los Alamos National Laboratory, Los Alamos, NM 87545, USA

E-mail: tanmoy@lanl.gov

Anosh Joseph

John von Neumann Institute for Computing, DESY, 15738 Zeuthen, Germany

E-mail: anosh.joseph@desy.de

Huey-Wen Lin

Department of Physics, University of Washington, Seattle, WA 98195

E-mail: hwlin@phys.washington.edu

Boram Yoon

Theoretical Division, Los Alamos National Laboratory, Los Alamos, NM 87545, USA

E-mail: boram@lanl.gov

We present a detailed analysis of statistical and systematic errors in the calculation of matrix elements of iso-vector scalar, axial and tensor charges between a neutron and a proton state. These analyses are being done on dynamical $N_f = 2 + 1 + 1$ HISQ configurations generated by the MILC Collaboration using valence clover fermions. Using ensembles at three values of the lattice spacing ($a = 0.12, 0.09, \text{ and } 0.06$ fm) and three values of the quark mass ($M_\pi \approx 310, 220$ and 130 MeV) we find that the estimates of the tensor charge are stable and it can be extracted with 5% precision with $O(10,000)$ measurements. We also find that higher statistics are needed to resolve the various uncertainties in the calculation of g_A and improve the signal in g_S , which with present data has large errors. A brief status report on the mixing and renormalization of novel operators contributing to nEDM is also given.

The 32nd International Symposium on Lattice Field Theory

23-28 June, 2014

Columbia University New York, NY

*Speaker.

†LA-UR-14-29293

1. Introduction

Precise calculations of the matrix elements of iso-scalar and iso-vector bilinear quark operators within nucleon states are needed to probe many exciting areas of the Standard Model (SM) and its extensions. In Ref. [1], we showed that new scalar and tensor interactions at the TeV scale could give rise to corrections at the 10^{-3} level in precision measurements of the helicity flip parts of the decay distribution of (ultra)cold neutrons (UCN). This sensitivity is reachable in experiments currently under construction and being planned. Even if these experiments see a signal, to constrain the allowed parameter space of beyond the SM (BSM) models, however, requires that matrix elements of isovector scalar and tensor bilinear quark operators are known to 10–20% accuracy. Similarly, in Ref. [2], we showed that to probe novel sources of CP violation in neutron electric dipole moment (nEDM), a combination of matrix elements of the iso-scalar and iso-vector tensor operators are needed to estimate the contribution of the quark EDM to the nEDM. Lattice calculations are well poised to provide these estimates with the desired precision.

In these proceedings, we present a detailed analysis of statistical and systematic errors in such calculations using 9 ensembles of 2+1+1 flavor HISQ lattices generated by the MILC collaboration [3]. The matrix elements are calculated using clover valence quarks. We examine the following sources of systematic errors – contribution of excited states, estimates of renormalization constants, finite volume and lattice discretization effects and dependence on quark mass. Three of these sources, statistics, contribution of excited states, and renormalization constants, affect the precision with which estimates from an individual ensemble are extracted. The other three, finite volume and lattice discretization effects and dependence on quark mass, require fits and extrapolations based on all the points. We examine the two classes of uncertainties separately.

2. Statistics

The MILC Collaboration [3] has generated ensembles of roughly 5500 trajectories of 2+1+1-flavor HISQ lattices at three values of light quark masses corresponding to $M_\pi \approx 310, 220, 130$ MeV at $a = 0.12, 0.09$ and 0.06 fm. We analyze configurations separated by 4–6 trajectories of the hybrid Monte Carlo evolution and discard the initial 300–500 trajectories for thermalization. The status of our analyses using these ensembles are summarized in Table 1. To increase the statistics, each configuration is analyzed using gaussian smeared sources in multiple locations displaced both in time and space directions to reduce correlations.

We performed the following statistical tests. The data for a given ensemble are divided into bins (by source point and configurations) and the Kolmogorov–Smirnov test is performed on quantities that have reasonable estimates configuration by configurations (iso-vector vector charge, value of 2-point function at a given time separation). While, this pairwise test showed that the sub-samples are consistent with being drawn from the same distribution, the mean values of observables fluctuated by up to 3σ . This variation is much larger than expected based on our bin size of over 1000 measurements. We do not find long tails in the distributions for any of the samples that could explain the fluctuation, but do see a variation in the sample distribution. One possible explanation is that the ensembles have not covered enough phase space and errors are consequently underestimated. Our overall conclusion is that a few thousand, and possibly $O(10,000)$ for the

Label	$L^3 \times T$	M_π MeV	$(M_\pi L)$	N_{cfgs}	$N_{\text{Measurements}}$	t_{sep}
a12m310	$24^3 \times 64$	305.3(4)	4.54	1013	8104	8, 9, 10, 11, 12
a12m220S	$24^3 \times 64$	218.1(4)	3.22	1000	24K (12K)	10 (8, 12)
a12m220	$32^3 \times 64$	216.9(2)	4.3	958	7664	8, 10, 12
a12m220L	$40^3 \times 64$	217.0(2)	5.36	1010	8080	10
a09m310	$32^3 \times 96$	312.7(6)	4.5	881	7058	10, 12, 14
a09m220	$48^3 \times 96$	220.3(2)	4.71	890	7120	10, 12, 14
a09m130	$64^3 \times 96$	128.2(1)	3.66	883	4824	10, 12, 14
a06m310	$48^3 \times 144$	319.3(5)	4.51	865	3460	16, 20
a06m220	$64^3 \times 144$	229.2(4)	4.25	430	1320	16, 20, 22, 24

Table 1: Description of the nine ensembles at $a = 0.12, 0.09, 0.06$ fm used in this study.

scalar charge, independent configurations with $O(32)$ measurements on each are needed to obtain estimates with $\leq 2\%$ errors.

3. Excited-State Contamination

Our current data show significant excited state contamination in both 2-point and 3-point functions. The goal is to extract all observables (charges, charge radii, form factors) by calculating matrix elements between ground-state nucleons. We address this by using smeared operators tuned to increase coupling to the ground state and suppress radially excited states. Second, as discussed in [4], we partially remove the remaining contamination by including one excited state in the analysis. Higher states are not included because with current statistics we are not able to resolve them, especially in the 3-point functions.

Denoting the first excited state mass by M_1 and coupling to our operator by \mathcal{A}_1 , the three-point function with source at $t_i = 0$, operator insertion at $t = t$ and sink at $t_f = t_{\text{sep}}$ can be written as

$$\begin{aligned}
\mathcal{C}_\Gamma^{(3),T}(t_i, t, t_f; \vec{p}_i, \vec{p}_f) &\approx |\mathcal{A}_0|^2 \langle 0|O_\Gamma|0\rangle e^{-M_0(t_f-t_i)} + |\mathcal{A}_1|^2 \langle 1|O_\Gamma|1\rangle e^{-M_1(t_f-t_i)} \\
&+ \mathcal{A}_0 \mathcal{A}_1^* \langle 0|O_\Gamma|1\rangle e^{-M_0(t-t_i)} e^{-M_1(t_f-t)} + \\
&+ \mathcal{A}_0^* \mathcal{A}_1 \langle 1|O_\Gamma|0\rangle e^{-M_1(t-t_i)} e^{-M_0(t_f-t)}. \tag{3.1}
\end{aligned}$$

The masses and amplitudes M_0 , M_1 , \mathcal{A}_0 , and \mathcal{A}_1 are obtained from fits to the two-point functions. The desired matrix element $\langle 0|O_\Gamma|0\rangle$ is then obtained by isolating $\langle 0|O_\Gamma|1\rangle$ and $\langle 1|O_\Gamma|1\rangle$. This requires doing calculations with multiple values of t and t_{sep} . Using the sequential source method, we carry out operator insertion at all values of t between the source and sink timeslices. The values of t_{sep} investigated are listed in Table 1. A nonlinear least-square fitter is then used to extract $\langle 0|O_\Gamma|0\rangle$ by fitting the data for all t_{sep} simultaneously using Eq. (3.1).

The $a = 0.12$ data for all three charges do not exhibit significant trends with respect to t_{sep} [4]. Simultaneous fits to $t_{\text{sep}} = 8, 10$ and 12 data are consistent with a fit to just the $t_{\text{sep}} = 10$ data. Consequently, in [4] we had concluded that $t_{\text{sep}} \geq 1.2$ fm is needed to control excited state contamination. The $a = 0.09$ and 0.06 data are much cleaner and show an increase in g_A with t_{sep} as illustrated in Fig. 1. On the other hand g_T continues to show very little sensitivity to t_{sep} . The errors

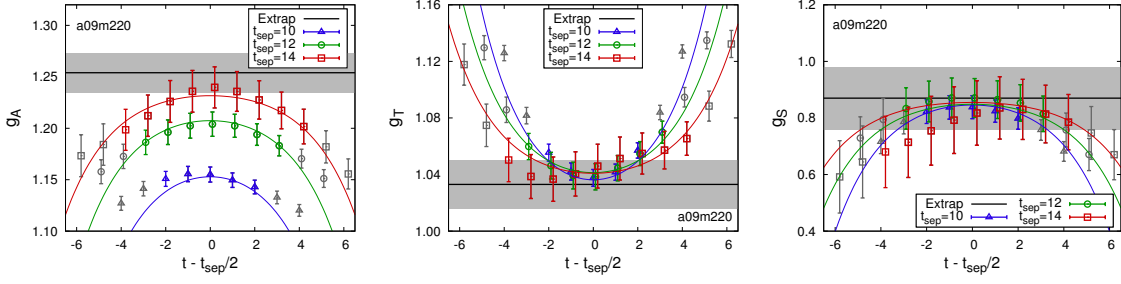


Figure 1: Fit using Eq.(3.1) to extract unrenormalized $g_{A,S,T}$ from the a09m220 ensemble data. The black line and the grey error band are the result of the simultaneous fit to the $t_{\text{sep}} = 10, 12$ and 14 data. The 3 colored lines are obtained from the simultaneous fit evaluated for each t_{sep} . To reduce excited-state contamination, the grey points on either side that are close to the source/sink timeslice, are not included in the fit.

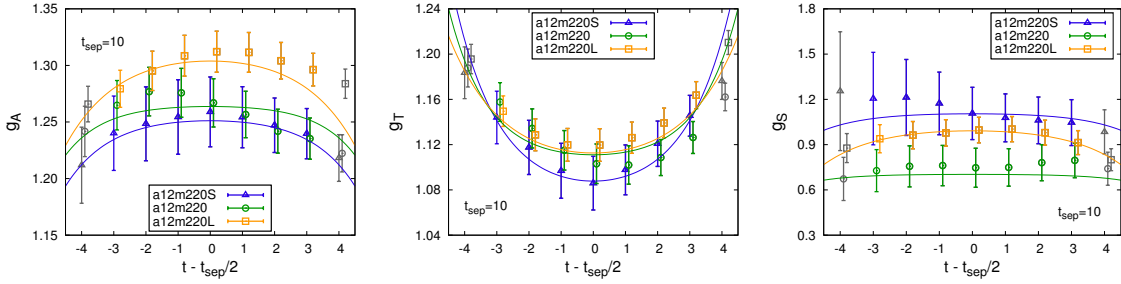


Figure 2: Study of finite volume effects in unrenormalized $g_{A,S,T}$ using fits to Eq.(3.1) on the $t_{\text{sep}} = 10$ data from the three a12m220 ensembles. Rest is same as in Fig. 1.

in g_S are too large to draw conclusions. Overall, trends in g_A data at weaker couplings imply that $t_{\text{sep}} \geq 1.5\text{fm}$ is needed to establish control over excited state contamination.

Our fits are biased by the smallest t_{sep} data because the statistics are the same for all t_{sep} , while errors increase with t_{sep} . For example, on the $a = 0.12\text{fm}$ ensembles, the statistical errors increase by about 40% with each unit increase in t_{sep} . This estimate scales with a , *i.e.*, on the $a = 0.06\text{fm}$ ensembles, the same fractional increase takes place every 2 units. Similarly, the errors increase by about 20% on lowering the light (u and d) quark masses by a factor of two, *i.e.*, going from $M_\pi = 310$ to 220 MeV ensembles. As an illustration, consider fits to $a = 0.09\text{fm}$ ensembles with $t_{\text{sep}} = 10, 12, 14$ shown in Fig. 1. The $t_{\text{sep}} = 10$ data make the largest contribution to the extraction of $\langle 0|O_\Gamma|0\rangle$ and $\langle 0|O_\Gamma|1\rangle$. The change between $t_{\text{sep}} = 10$ and 12 contributes to fixing $\langle 1|O_\Gamma|1\rangle$. For $t_{\text{sep}} = 14$ data to contribute at the same level, its statistics should be 3–4 times that of $t_{\text{sep}} = 10$ data.

4. Finite Volume Effects

The results of our finite volume study using the a12m220 ensembles with volumes $24^3, 32^3$ and 40^3 (corresponding $M_\pi L = 3.22, 4.3$ and 5.36) are shown in Fig. 2. The g_A data show significant increase with volume, while the g_T data show saturation between the $M_\pi L = 4.3$ and 5.36 data. The g_S data are again too noisy. Our conclusion is that lattices with $M_\pi L \geq 5$ are needed to control finite volume effects unless we can reliably model extrapolation in lattice volume.

5. Non-perturbative Renormalization

We use the RI-sMOM scheme to calculate the renormalization constants of the bilinear quark operators [5]. Details of the method and our implementation were presented in [4]. The most important issue, especially when using smeared lattices, was demonstrating the presence of a window in momentum q , $\Lambda_{QCD} \ll q \ll c/a$ with c an *a priori* unknown number of $O(1)$, where lattice artifacts are expected to be small. Sufficiently close to the continuum limit where perturbation theory works, a test of whether such a window exists is that Z_S and Z_T in the RI-sMOM (or any lattice) scheme should show a q^2 dependence given by the anomalous dimensions of these operators along with a weaker dependence from the running of α_s , while Z_A should only show the latter. Converting estimates obtained from within such a window in q^2 in the RI-sMOM scheme to the $\overline{\text{MS}}$ scheme used in phenomenology and run to some fixed scale, say $\mu = 2 \text{ GeV}$, should give estimates independent of q^2 . Based on our analyses at the three lattice spacings (see [4] for details) our conclusions are: there is evidence of such behavior, *i.e.*, a window, in Z_A and Z_T , but not in Z_S even on $a = 0.06 \text{ fm}$ ensembles. Lacking a convincing demonstration of a window, we have defined a procedure that will extrapolate to the right continuum limit [4] and have been conservative in estimating errors, however, we recommend a further study at various a , in particular for Z_S .

6. Combined fits in lattice volume, spacing and quark mass

Having discussed the first class of uncertainties that affect individual data points, we now discuss extrapolations in lattice spacing and volume, and the quark mass. It is very hard to generate dynamical lattices with fixed quark masses (fixed M_π) and lattice volumes (fixed $M_\pi L$) at multiple a in order to take the continuum limit along a line of constant physics. Similarly, it is not easy to hold the lattice volume and a constant and vary the quark mass to study the chiral behavior. Our best option is to do a combined fit in a , M_π and $M_\pi L$ to obtain physical estimates. The second challenge is choosing the extrapolation ansatz in each of these three variables — we have to compromise between the number of free parameters included and the number and quality of data points. In Fig. 3 we show such a fit keeping only the leading order terms in each of the three variables,

$$g(a, M_\pi, M_\pi L) = g^{\text{physical}} + \alpha a + \beta M_\pi^2 + \gamma e^{-M_\pi L}. \quad (6.1)$$

In Fig. 3, note that the errors in individual points vary significantly. As a result, with 9 data points, this ansatz with 4 free parameters is the most extensive we can explore.

Fig. 3 summarizes the trends mentioned before. Removing excited state contributions and doing finite volume and chiral extrapolations all increase g_A towards the experimental value. Data for g_T show almost no dependence on a , M_π or $M_\pi L$ and give $g_T = 1.06(0.06)$. We consider this estimate reliable. Statistical errors are too large to draw conclusions about g_S .

Prognosis for the future: Based on current analyses, we conclude that with current ensembles and $O(10,000)$ measurements, we can extract g_T with about 2% errors on each point, and $\approx 5\%$ uncertainty in the extrapolated value. To extract g_A with similar precision will require $O(2000)$ configurations at three values of $a \leq 0.1 \text{ fm}$, $M_\pi L \geq 5$ and $O(24)$ measurements on each configuration to get statistically significant data for $1.2 \leq t_{\text{sep}} \leq 1.6 \text{ fm}$. Estimates of g_S with similar precision will require an order of magnitude more measurements.

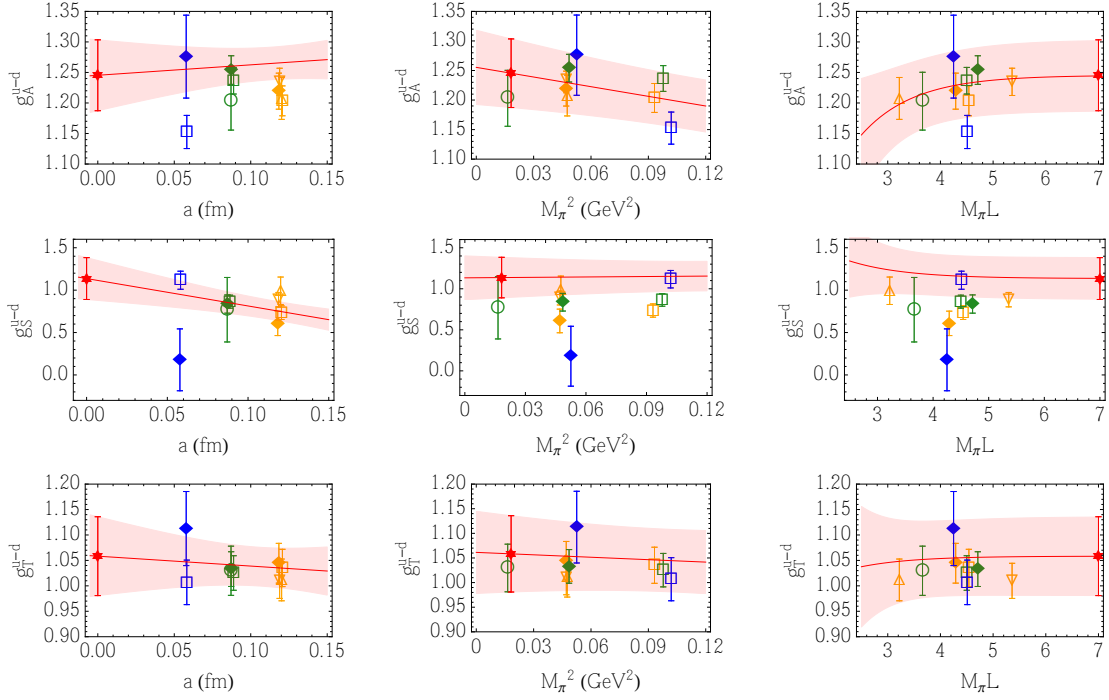


Figure 3: Results of combined fits in a , M_π and $M_\pi L$ to obtain the physical results for the renormalized charges using the ansatz given in Eq. (6.1). Iso-vector charges are labeled as g^{u-d} .

7. BSM contributions to Neutron Electric Dipole Moment

Lattice calculations of matrix elements of effective quark EDM and chromo EDM operators within a neutron state to probe BSM theories were initiated in [2]. The simpler is the quark EDM which is an extension of g_T but matrix elements of both isovector and isoscalar tensor operators are needed. One, therefore, has to evaluate and control the signal in the disconnected diagrams [6]. We also analyze operator mixing and renormalization in 1-loop perturbation theory. For brevity, operators that vanish by the equations of motion are included by introducing the field combinations:

$$\psi_E \equiv (iD^\mu \gamma_\mu - m)\psi, \quad D_\mu = \partial_\mu - igA_\mu^a T^a - ie_\psi A_\mu^{(\gamma)} \quad (7.1)$$

$$\bar{\psi}_E \equiv -\bar{\psi}(i\overleftarrow{D}^\mu \gamma_\mu + m), \quad \overleftarrow{D}_\mu = \overleftarrow{\partial}_\mu + igA_\mu^a T^a + ie_\psi A_\mu^{(\gamma)}. \quad (7.2)$$

In terms of these fields, the operators we study are given in Table 2. The pattern of mixing of the dimension 5 operators under renormalization that needs to be calculated is given in Table 3. Papers containing 1-loop results for the mixing and a first estimate of the quark EDM are being prepared.

Acknowledgments

We thank the MILC Collaboration for sharing the 2+1+1 HISQ ensembles. Simulations were performed using the Chroma software suite [7] on LANL Institutional Computing, the USQCD Collaboration facilities funded by the U.S. DoE; XSEDE supported by NSF grant number OCI-1053575; and a DOE grant at NERSC. RG, TB and BY are supported by DOE grant DE-KA-1401020 and the LDRD program at LANL. HL was supported in part by DOE grant No. DE-FG02-97ER4014. The nEDM calculations are being done with V. Cirigliano and E. Mereghetti.

$O^{(3)} = iP = \bar{\psi}i\gamma_5\psi$ $O_1^{(4)} = G\tilde{G} = \frac{1}{2}\varepsilon^{\mu\nu\alpha\beta}G_{\mu\nu}^aG_{\alpha\beta}^a$ $O_2^{(4)} = \partial \cdot A = \partial_\mu(\bar{\psi}\gamma^\mu\gamma_5\psi)$ $O_3^{(4)} = imP = m\bar{\psi}i\gamma_5\psi$ $O_4^{(4)} = F\tilde{F} = \frac{1}{2}\varepsilon^{\mu\nu\alpha\beta}F_{\mu\nu}F_{\alpha\beta}$	$O_1^{(5)} = C = \frac{ig}{2}\bar{\psi}(\sigma^{\mu\nu}\gamma_5 + \gamma_5\sigma^{\mu\nu})G_{\mu\nu}\psi$ $O_2^{(5)} = i\partial^2P$ $O_3^{(5)} = E = \frac{ie}{2}\bar{\psi}(\sigma^{\mu\nu}\gamma_5 + \gamma_5\sigma^{\mu\nu})F_{\mu\nu}\psi$ $O_4^{(5)} = mF\tilde{F}$ $O_5^{(5)} = mG\tilde{G}$ $O_6^{(5)} = m\partial \cdot A$ $O_7^{(5)} = m^2iP$ $O_8^{(5)} = iP_{EE} = i\bar{\psi}_E\gamma_5\psi_E$ $O_9^{(5)} = \partial \cdot A_E = \partial_\mu[\bar{\psi}_E\gamma^\mu\gamma_5\psi + \bar{\psi}\gamma^\mu\gamma_5\psi_E]$ $O_{10}^{(5)} = A_\partial = \bar{\psi}\gamma_5\overleftarrow{\partial}\psi_E - \bar{\psi}_E\overleftarrow{\partial}\gamma_5\psi$ $O_{11}^{(5)} = A_{A^{(\gamma)}} = ie\left(\bar{\psi}A^{(\gamma)}\gamma_5\psi_E - \bar{\psi}_EA^{(\gamma)}\gamma_5\psi\right)$
---	--

Table 2: Operators of dimension 3, 4 and 5 needed in the nEDM calculation.

	C	∂^2P	E	$mF\tilde{F}$	$mG\tilde{G}$	$m\partial \cdot A$	m^2P	P_{EE}	$\partial \cdot A_E$	A_∂	$A_{A^{(\gamma)}}$
C	Z_C	X	X	X	X	X	X	X	X	X	X
∂^2P	0	Z_P	0	0	0	0	0	0	0	0	0
E	0	0	Z_T	0	0	0	0	0	0	0	0
$mF\tilde{F}$	0	0	0	$Z_m^{-1}Z_{F\tilde{F}}$	0	0	0	0	0	0	0
$mG\tilde{G}$	0	0	0	0	$Z_m^{-1}Z_{G\tilde{G}}$	X	0	0	0	0	0
$m\partial \cdot A$	0	0	0	0	0	$Z_m^{-1}Z_{\partial A}$	0	0	0	0	0
m^2P	0	0	0	0	0	0	Z_m^{-1}	0	0	0	0
P_{EE}	0	0	0	0	0	0	0	X	X	X	0
$\partial \cdot A_E$	0	0	0	0	0	0	0	0	X	0	0
A_∂	0	0	0	0	0	0	0	X	X	X	0
$A_{A^{(\gamma)}}$	0	0	0	0	0	0	0	0	0	0	X

Table 3: Mixing due to QCD of the dimension-5 operators. Non-zero entries need to be determined.

References

- [1] T. Bhattacharya, *et al.*, Phys.Rev. **D85** (2012) 054512.
- [2] T. Bhattacharya, *et al.*, PoS (LATTICE 2012), 179 (2012) and PoS (LATTICE 2013) 299 (2103).
- [3] A. Bazavov, *et al.*, MILC Collaboration, Phys. Rev. **D87** (2013) 054505.
- [4] T. Bhattacharya, *et al.*, Phys.Rev. **D89** (2014) 094502.
- [5] G. Martinelli, *et al.*, Nucl.Phys. **B445** (1995) 81; C. Sturm, *et al.*, Phys.Rev. **D80** (2009) 014501.
- [6] B. Yoon, *et al.*, These proceedings: PoS (LATTICE 2014), 141 (2014).
- [7] R. Edwards, B. Joo, Chroma Software System for LQCD, Nucl. Phys. Proc. Suppl. **140** (2005) 832